The XIII International Conference on the Physics of Non-Crystalline Solids

Preparation of mesoporous V_2O_5@TiO_2 composites with enhanced photoactivity for gaseous benzene degradation

Chunxia Zhao, Subo Feng, Wen Chen*, Xiaoyu Li, Yanbao Song, Jinqiao Cao

State Key Laboratory of Advanced Technology for Materials Synthesis and Processing, School of Material Science and Engineering, Wuhan University of Technology, Wuhan 430070, P.R.China

Abstract

Mesoporous V_2O_5@TiO_2 composites were fabricated by an ultrasonic method with V_2O_5 sol as the guest precursor. The prepared materials were characterized by powder X-ray diffraction, field emission-scanning electron microscopy, transmission electron microscope, X-ray photoelectron spectroscopy, UV-Vis spectroscopy and nitrogen sorption analysis. The results indicated that V_2O_5 nanoparticles dispersed well on/into the porous structure of TiO_2 matrix. The composites presented typical IUPAC IV isotherms with type H_2 hysteresis loops, revealing the mesoporous structure. It was observed that V_2O_5 loading led to red shift of the absorption edge to 540 nm and reduced the band gap < 3.0 eV. The V_2O_5@TiO_2 composites with V/Ti molar ratio of 0.1 exhibited outstanding degradation efficiency of gaseous benzene.

Keywords: Mesoporous composites; V_2O_5; TiO_2; photoactivity; benzene; degradation

1. Introduction

Recently, indoor air quality problems have drawn increasing attention since people spend more than 80% of their time in an indoor environment. Indoor air pollutants, however, are inevitable because industrial processes and domestic activities produce pollutants from combustion byproducts, construction materials, office equipments, nearby traffic vehicles and etc. [1-4]. The major indoor air pollutants are volatile organic compounds (VOCs) composed of BTEX (benzene, toluene, ethylbenzene, and o-xylene) which are known to

* Corresponding author. Tel.: +86-27-87651107; Fax: +86-27-87760129.
E-mail address: chenw@whut.edu.cn.

be toxic and carcinogenic [5, 6]. Photocatalytic oxidation has been proven to be a promising technology for air purification and pollution control. Typically, TiO_2, which generates highly reactive radical species such as $\cdot OH$ and $\cdot O_2^-$, has been widely used and investigated due to its inexpensiveness, strong oxidizing power, non-toxicity and long-term photostability [7]. Unfortunately, the recombination ratio of photo-induced electrons and positive holes produced from the interior of pure TiO_2 under the irradiation of UV light is so high that the photocatalytic efficiency of TiO_2 to degrade pollutants is greatly decreased. Therefore, considerable efforts have been made to modify TiO_2 material in order to broaden the photo-response of TiO_2-based photocatalysts and enhance the photocatalytic activity. V_2O_5 modified TiO_2 is generally recognized as a potential catalyst and considered to be an effective approach to this problem [8-10].

In this work, we synthesized mesoporous TiO_2 based on the "acid-base pairs" theory [11] and prepared the $V_2O_5@TiO_2$ composites using an ultrasonic method with mesoporous TiO_2 as the host and V_2O_5 sol as the guest precursor. Then, characterization and the photocatalytic degradation efficiency of gaseous benzene pollutant with $V_2O_5@TiO_2$ composites were investigated.

2. Experimental

2.1. Preparation of mesoporous V_2O_5/TiO_2 composites

Mesoporous TiO_2 host (MT) was prepared based on the "acid-base pairs" theory [11]. In a typical synthesis, 3.6 g tetrabutyl titanate (TBOT, 98%) and 0.4 g titanium tetrachloride ($TiCl_4$, 98%) were added to a clear sol containing 20 mL ethanol (C_2H_5OH, 99.7%) and 1 g surfactant P123 ($EO_{20}PO_{70}EO_{20}$, Mav=5800, Aldrich). After vigorous stirring for 4 h, the resulting solution was poured into Petri dishes for aging for 24 h. Then the obtained product was picked off from Petri dishes and calcined at 653 K for 5 h to remove the organic components. All chemicals were used as received without further purification.

V_2O_5 sol was prepared using an ice-bath by dispersing V_2O_5 powder (0.545 g) in a solution of H_2O_2 (50 mL) at 273 K under continuous stirring. Then, the prepared mesoporous TiO_2 was dispersed into the fresh V_2O_5 sol. After subjecting to ultrasound treatment for 3 h, the mixture was filtrated and the collected product was calcined at 653 K for 3 h to obtain the V_2O_5 loaded mesoporous TiO_2 composites, named as $V_2O_5@TiO_2$. $V_2O_5@TiO_2$ composites with different amount of V_2O_5 loading were named as xVT, where x (0.1, 0.2 and 0.3) refers to the V/Ti molar ratio.

2.2. Characterization

XRD patterns were collected on X'Pert pro diffractometer (PANalytical, The Netherlands) using Ni-filtered CuKα radiation (λ= 1.5418 Å). FE-SEM was carried out on a JEOL JSM-6330F microscope operating at 20 kV. TEM images of the samples were recorded on a JEOL JEM-2100F microscope operating at 200 kV. Nitrogen sorption isotherms were measured using an ASAP2020 adsorption analyzer (Micromeritics) at 77 K. The surface area and the pore size distribution were estimated by multipoint Brunauer-Emmett-Teller (BET) method and BJH method, respectively. Total pore volume was determined from the amount of nitrogen adsorption at $P/P_0 \approx 0.96$. Diffusive reflectance UV-vis absorption spectra were recorded on a UV-2550 UV-Vis spectrophotometer.

2.3. Photocatalytic degradation of gaseous benzene

The photocatalytic activity of the synthesized samples was evaluated by photo-decomposition of gaseous benzene, conducted in a hermetic stainless steel chamber (5 L). A lamp with the wavelength centered at 365 nm was installed on the bracket in the chamber. The catalyst (0.4 g sample) was dispersed as a thin layer over

a glass vessel with the total area of 180 cm^2. 2 μL of benzene was diluted in air with the starting concentration kept at 480 mg/m^3 for all experimental cases. The total pressure of the system was kept at 133.2 kPa, and the initial partial pressure of benzene was 0.046 Pa. Simultaneous concentration determination of benzene and carbon dioxide was performed with an online gas chromatograph equipped with an aflameionization detector, a thermal conductivity detector, and a porapak R column. The reaction temperature of the photocatalytic system was held at 393 K. Photocatalytic measurements were performed on a Gas Chromatography (Shanghai Chenhua Technology Corp, Ltd.).

3. Results and discussion

3.1. Structure characterization

Fig. 1 shows the XRD patterns of the as-made mesoporous TiO$_2$ and xVT. The diffraction peaks of mesoporous TiO$_2$ at 2θ = 25.21°, 37.53°, 47.87°, 53.95°, 54.86° and 62.37° corresponding to anatase (101), (004), (200), (105), (211) and (204) planes suggest an anatase phase of TiO$_2$. It is observed that there is no significant change in XRD patterns at corresponding diffraction angles of anatase phase in xVT, indicating that TiO$_2$ phase does not change with V$_2$O$_5$ loading. In addition, some narrow diffraction peaks with low intensities are found with increasing of V$_2$O$_5$ loading, such as 0.3VT, which could be assigned to V$_2$O$_5$ particles.
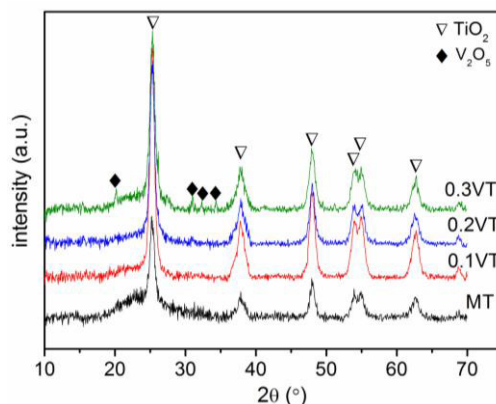

Fig. 1. XRD patterns of mesoporous TiO$_2$ and xVT.

The FE-SEM images of mesoporous TiO$_2$ and xVT along with EDS are shown in Fig.2. It is demonstrated that the MT host materials are consisted of a large number of nanoparticles with the diameter of 10-20 nm. By comparison, the morphology of xVT was preserved well after V$_2$O$_5$ loading. The nanoparticles size does not change much and no clear aggregation is exhibited in these images of the composites. In addition, EDS analysis of xVT reveals the presence of Ti, O and V traces. All these results could be assigned to the good dispersion of V$_2$O$_5$ nanoparticles on/into the TiO$_2$.

Fig. 3 shows the TEM images of the mesoporous TiO$_2$ and 0.1VT samples. The TiO$_2$ particles of MT were uniformed with a size of around 10-20 nm. The lattice fringes of d = 0.35 nm matches that of the (101) crystallographic planes of anatase TiO$_2$, agreeing with the XRD results above. Compared with the mesoporous TiO$_2$, 0.1VT maintained the initial morphology and no clear aggregations were observed. The crystal structure did not change much, indicating that V$_2$O$_5$ well dispersed on/into the TiO$_2$.

Fig. 4 represents the XPS spectra of the Ti 2p, V 2p and O 1s regions for the 0.1VT sample. The Ti 2p region (Fig. 4a) is composed of two symmetrical peaks at around 459.5 and 465.1 eV, corresponding to the

Ti^{4+} in the 0.1VT sample [16]. The spectrum of V 2p peaks (Fig. 4b) over the sample is well de-convoluted by two peaks at 524.9 (V2p1/2) and 517.9 eV (V 2p3/2), indicating that V exists as the V^{5+} form [16-18]. The O 1s peak can be deconvoluted into two peaks at about 529.7 and 531.8 eV (Fig. 4c). The peak at around 529.7 eV is associated to lattice oxygen arising from vanadium and titanium lattices, and the binding energy of 531.8 eV can be attributed to surface OH$^-$ group, which is similar to that found on transition metals hydroxides and oxides. The broad feature of V 2p and O 1s peaks in the V$_2$O$_5$@TiO$_2$ composites might due to the high dispersion of V$_2$O$_5$ nanoparticles on TiO$_2$ [19-23].
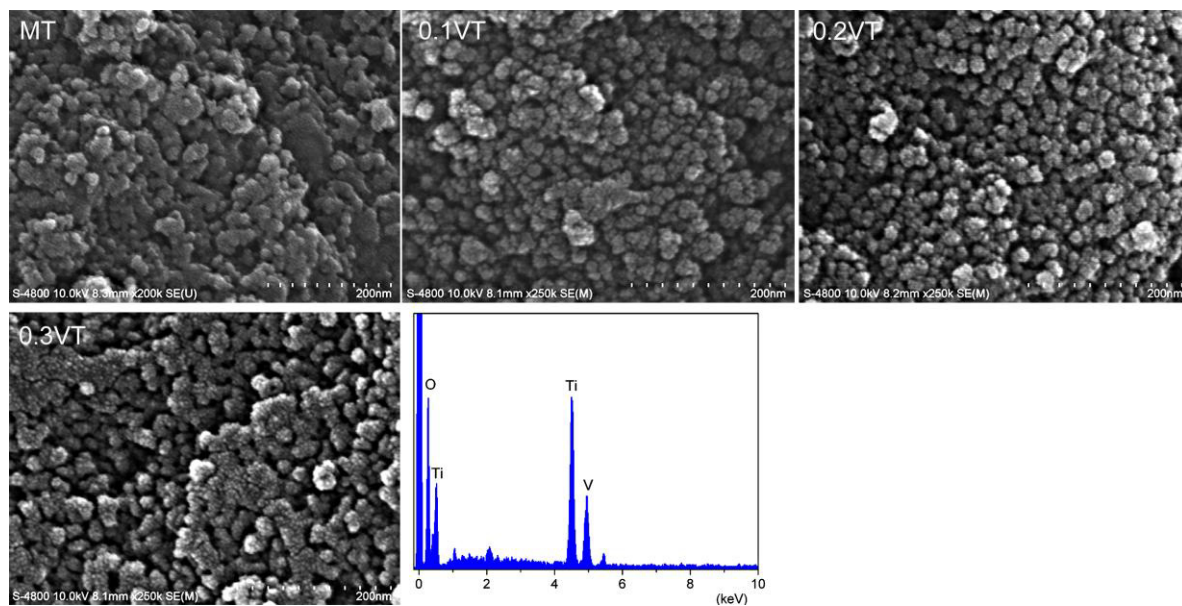

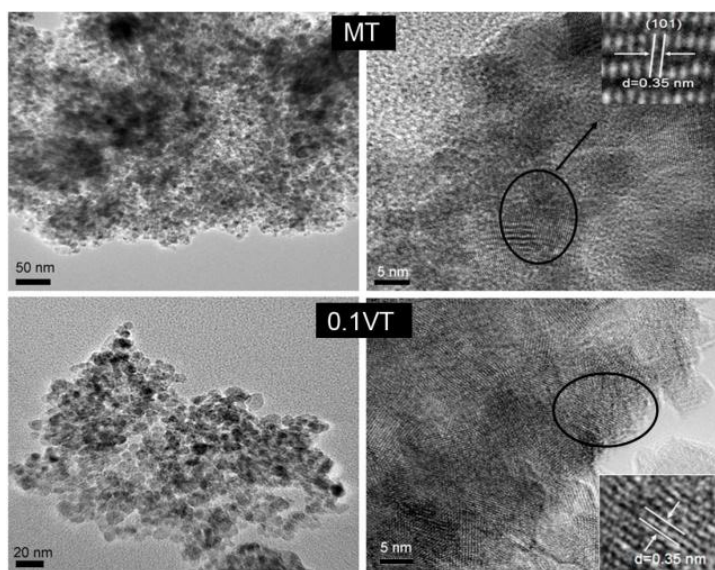Fig. 2. FE-SEM images of MT and *x*VT and EDS.
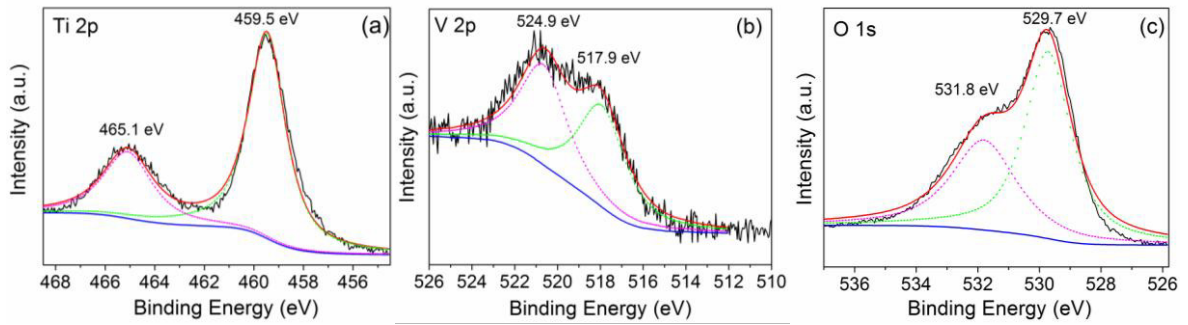

Fig. 3. TEM images of MT and 0.1VT.

Fig. 4. Ti 2p (a), V 2p (b) and O 1s (c) XPS high resolution spectra of the 0.1VT sample.

In order to investigate the surface area and pore structure of the samples, nitrogen adsorption/desorption measurements were carried out. The results are shown in Fig.5. In Fig. 5A, N_2 sorption isotherms for all the samples exhibited the type IV isotherms with type H_2 hysteresis loops according to IUPAC classification, indicating the presence of mesopores. When V_2O_5 nanoparticles were introduced into TiO_2 host, the adsorbed N_2 volume became smaller as V_2O_5 amount increased. Moreover, from the change of pore size distributions (PSDs), shown in Fig. 5B, monodispersed PSD was observed for 0.1VT with a diameter of ~ 6.1 nm, which is similar to the reported results [24-26]. For higher V_2O_5 addition, a large collapse of pore structure was observed. BET specific surface area was decreased from 167.2 (MT), 139.9 (0.1VT), 133.5 (0.2VT) to 129.6 (0.3VT) m^2/g with the increase of V_2O_5. From the above structural analysis, therefore, it was confirmed that V_2O_5 nanoparticles were incorporated into the mesoporous structure of TiO_2 matrix.
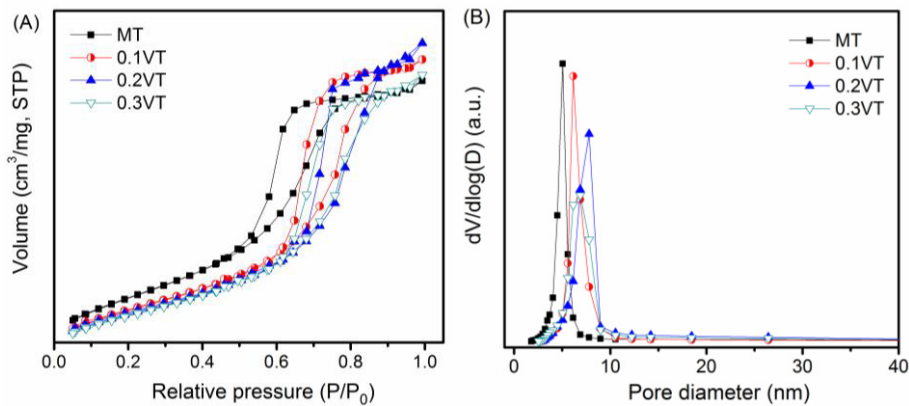

Fig.5. Nitrogen sorption isotherms (A) and pore size distributions (B) of MT and xVTs.

The UV-Vis spectra of mesoporous TiO_2 and $V_2O_5@TiO_2$ composites are presented in Fig. 6A. Compared to mesoporous TiO_2, xVT samples resulted in a substantial red shift of the absorption edge (to 544 nm) and exhibited a great enhancement of absorption intensity in the visible light region. Particularly, 0.1VT shows a very strong absorption peak in the UV region. It could be attributed to that the coupling of TiO_2 with V_2O_5 having different Fermi levels might induce semiconductor energy band bending at the junction and shift the absorption band of the titanium oxide towards the visible light region. The band gap of the mesoporous TiO_2 and xVT is obtained by the following equation using the data of optical absorption:

$$\alpha h\nu = A(\ h\nu - E_g\ )^{n/2}$$

Where α, ν, A E_g and n are absorption coefficient, light frequency, proportionality constant, band gap and exponent, respectively [27]. The band-gap energy of *x*VT are lower than that of mesoporous TiO_2 leading to the red shift as shown in Fig. 6B. The shift can be assigned to the V_2O_5 loading. The value of the band gap for 0.1VT, 0.2VT and 0.3VT are 3.0, 2.7 and 2.5 eV, respectively. They are much lower than that of MT (3.1 eV). Thus, it is proposed that V_2O_5 loading could expand the absorption range and reduce the band gap of TiO_2 and then might influence the photocatalytic activity of TiO_2 due to the semiconductor energy band bending at the junction.
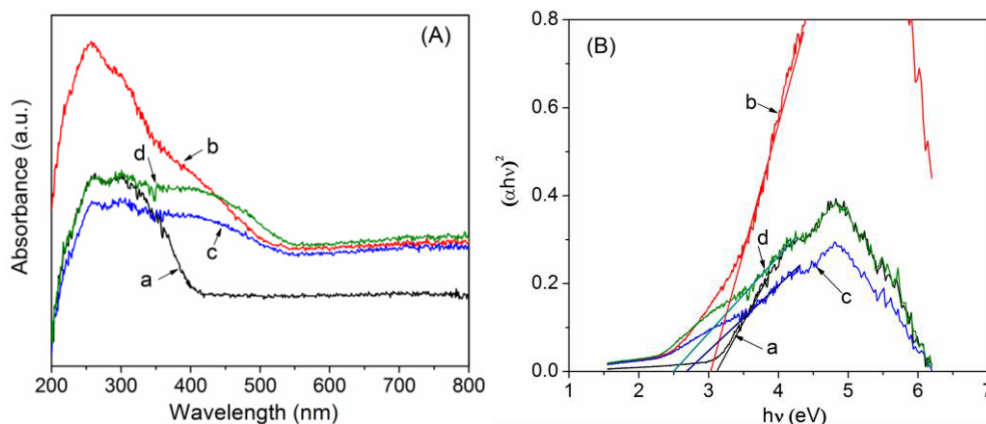

Fig. 6. UV-vis spectra (A) and curve of $(\alpha h\nu)^2$ vs. hν (B) of MT (a) and *x*VTs (b-0.1VT, c-0.2VT, d-0.3VT).

3.2. Photocatalytic activity

Fig. 7A presents the results of photo-degradation of benzene under UV-vis light illumination. It shows that all the samples can remove more than 66% of benzene after 80 min UV-vis irradiation. It reveals that all the prepared catalysts have considerable benzene removal performance under UV-Vis light illumination in short time. Particularly, 0.1VT sample shows the best removal efficiency of benzene at ~90%. Fig. 7B shows the plots of the changes in CO_2 concentration during degrading benzene pollutants. The amount of CO_2 is an indication for photocatalytic activity of catalysts, suggesting the efficiency of complete photodegradating benzene to CO_2 production. It is observed that 0.1VT sample exhibits significantly more amount of decomposed CO_2. It means that although both MT and 0.1 VT show similar benzene removal amount as in Fig. 7A, 0.1 VT demonstrates much complete degradation of benzene to CO_2. Hence, 0.1 VT sample has the highest degradation efficiency of gaseous benzene.

It is proposed that there could be mainly two competing factors that affect the photocatalytic behavior. The electronic structure change of TiO_2 due to V_2O_5 loading may be a dominant factor. According to the UV-vis spectra, 0.1VT has substantial red-shift of the absorption edge and lower band gap energy, which could induce more photo-generated electrons and holes to participate in the photocatalytic reactions. Meanwhile, V_2O_5 loading can lead to the formation of recombination centers which appeared as gap states in the present experiment. As a result, the yield and recombination of photo-induced electron-hole pairs formed two contradicted factors that determined photocatalysis. In the case of 0.1VT, the contribution from the electronic structure change with V_2O_5 loading might dominate the total photocatalytic activity. However, further increase of the V_2O_5 loading leads to the noticeable decrease of surface area of the composites and then causes visible reduction in photocatalytic activity [28].
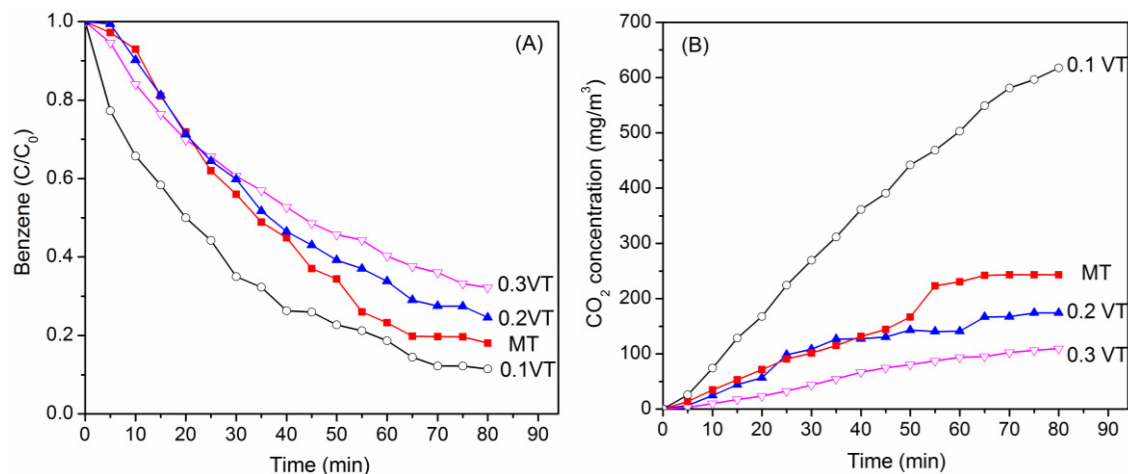
Fig. 7. Plots of the decrease in benzene concentration (A) and the increase in CO_2 concentration (B) vs. irradiation time during the photocatalytic degradation of benzene.

4. Conclusions

$V_2O_5@TiO_2$ composites, which were successfully fabricated via ultrasound method, were able to well retain the mesoporous structure and particle morphology of the mesoporous TiO_2 host. The calculated band-gap energy of $V_2O_5@TiO_2$ composites were lower than that of TiO_2, indicating that V_2O_5 loading could expand the absorption range and reduce the band gap of TiO_2. This was considered to mainly act as recombination centers for the UV-light induced photocatalytic course. The yield and recombination of the photoinduced electrons and holes were two competing factors that determined the UV-photocatalytic activity, leading to moderate V_2O_5 loading amount. When the molar ratio of V/Ti is 0.1, the composites exhibit great improvement of photocatalytic activity on gaseous benzene degradation.

Acknowledgements

References

[1] L. Zou, Y. Luo, M. Hooper, E. Hu. *Chem. Eng. Process.* **45**(2006): 959-964.
[2] A.P. Jones. *Atmos. Environ*. **33**(1999): 4535-4564.
[3] F.B. Li, X.Z. Li, C.H. A, S.C. Lee, M.F. Hou. *Chemosphere* **59**(2005): 787-800.
[4] C.H. Ao, S.C. Lee. *Chem. Eng. Sci*. **60**(2005): 103-109.
[5] S.B. Kim, S.C. Hong. *App. Catal. B: Environ*. **35**(2002): 305-315.
[6] M.R.Van Winkle, P.A. Scheff. *Indoor Air* **11**(2001): 49-64.
[7] T. Ohno, S. Izumi, K. Fujhara, Y. Masaki, M. Matsumura. *J. Phys. Chem. B* **104**(2000): 6801-6803.
[8] A. Houas, H. Lachheb, M. Ksibi, E. Elaloui, C. Guillard, J.M. Herrmann. *Appl. Catal. B: Environ*. **31**(2001) : 145-157.

[9] M. Vautier, C. Guillard, J.M. Hermann. *J. Catal*. **201**(2001): 46-59.

[10] M.R. Hoffmann, S.T. Martin, W. Choi, D.W. Bahnemann. *Chem. Rev*. **95**(1995): 69-96.

[11] B. Tian, X. Liu, B. Tu, C. Yu, J. Fan, L. Wang, S. Xie, G.D. Stucky, D.Y. Zhao. *Nat. Mater*. **2**(2003): 159-163.

[12] H. Kumazawa, M. Inoue, T. Kasuya. *Ind. Eng. Chem. Res*. **42**(2003): 3237-3274.

[13] D.Hornero-Mendez, M.I. Minguez-Mosquera. *J. Agric. Food Chem*. **49**(2001): 3584-3588.

[14] J.G. Yu, H.G. Yu, B. Cheng, X.J. Zhao, J.C. Yu and W.K. Ho. *J. Phys. Chem. B* **107**(2003): 13871-13879.

[15] B.M. Reddy, K.N. Rao, G.K. Reddy, P. Bharali. *J. Mol. Catal. A: Chem.* **253**(2006): 44-51.

[16] J. Haber, J. Stoch. *React. Kinet.Catal. Lett*. **9**(1978):319-323.

[17] G. Hopfengärtner, D. Borgmann, I. Rademacher, G. Wedler, E. Hums, G.W. Spitznagel. *J. Electron Spectrosc. Relat. Phenom.* **63**(1993): 91-116.

[18] J. Mendialdua, R. Casanova, Y. Barbaux. *J. Electron Spectrosc. Relat. Phenom.* **71**(1995): 249-261.

[19] S. Lars, T. Andersson. *Catal. Lett*. **7**(1990): 351-358.

[20] E.S. Zhan, Y. Li, J.L. Liu, X.M. Huang, W.J. Shen. *Catal. Comm*. **10**(2009): 2051-2055.

[21] S. Yuan, Q.R. Sheng, J.L. Zhang, H. Yamashita, D.N. He. *Micropor. Mesopor. Mater*. **110**(2008) : 501-507.

[22] Y.D. Hou, X.C. Wang, L. Wu, X.F. Chen, Z.X. Ding, X.X. Wang, X.Z. Fu . *Chemosphere* **72**(2008):414-421.

[23] M. A. Bañares, L. J. Alemany, M.C. Jiménez, M.A. Larrubia, F. Delgado, M. L. Granados, A. Martínez-Arias, J.M. Blasco, J. Luís, G. Fierro. *J. Solid State Chem*. **124**(1996):69-76.

[24] H. Yoshitake, T. Tatsumi. *Chem. Mater*. **15**(2003):1695-1702.

[25] L. Yu, C.X. Zhao, X. Long, W. Chen. *Micropor. Mesopor. Mater*. **126**(2009): 58-64.

[26] R. Liu, Y. Ren, Y. Shi, F. Zhang, L. Zhang, B. Tu, D. Zhao. *Chem. Mater*. **20**(2008): 1140-1146.

[26] Y. Segura, L. Chmielarz, P. Kustrowski, P. Cool, R. Dziembaj, E. F. Vansant. *J. Phys. Chem. B* **110**(2006): 948-955.

[27] X.P. Lin, F.Q. Huang, W.D. Wang, Y.J. Xia, Y.M. Wang, M.L. Liu, J.L. Shi. *Catal. Comm*. **9** (2008): 572-576.

[28] B. Liu, X. Wang, G. Cai, L. Wen, Y. Song, X. Zhao. *J. Hazard. Mater*. **169**(2009): 1112-1118.